



## Quantum interface of an electron and a nuclear ensemble

Gangloff, D. A.; Éthier-Majcher, G.; Lang, C.; Denning, E. V.; Bodey, J. H.; Jackson, D. M.; Clarke, E.; Hugues, M.; Gall, C. Le; Atatüre, M.

*Published in:*  
Science

*Link to article, DOI:*  
[10.1126/science.aaw2906](https://doi.org/10.1126/science.aaw2906)

*Publication date:*  
2019

*Document Version*  
Peer reviewed version

[Link back to DTU Orbit](#)

*Citation (APA):*  
Gangloff, D. A., Éthier-Majcher, G., Lang, C., Denning, E. V., Bodey, J. H., Jackson, D. M., Clarke, E., Hugues, M., Gall, C. L., & Atatüre, M. (2019). Quantum interface of an electron and a nuclear ensemble. *Science*, 364(6435), 62-66. <https://doi.org/10.1126/science.aaw2906>

---

### General rights

Copyright and moral rights for the publications made accessible in the public portal are retained by the authors and/or other copyright owners and it is a condition of accessing publications that users recognise and abide by the legal requirements associated with these rights.

- Users may download and print one copy of any publication from the public portal for the purpose of private study or research.
- You may not further distribute the material or use it for any profit-making activity or commercial gain
- You may freely distribute the URL identifying the publication in the public portal

If you believe that this document breaches copyright please contact us providing details, and we will remove access to the work immediately and investigate your claim.

Cite as: D. A. Gangloff *et al.*, *Science*  
10.1126/science.aaw2906 (2019).

# Quantum interface of an electron and a nuclear ensemble

D. A. Gangloff<sup>1\*†</sup>, G. Éthier-Majcher<sup>1\*‡</sup>, C. Lang<sup>1</sup>, E. V. Denning<sup>1,2</sup>, J. H. Bodey<sup>1</sup>, D. M. Jackson<sup>1</sup>, E. Clarke<sup>3</sup>, M. Hugues<sup>4</sup>, C. Le Gall<sup>1</sup>, M. Atatüre<sup>1†</sup>

<sup>1</sup>Cavendish Laboratory, University of Cambridge, JJ Thomson Avenue, Cambridge CB3 0HE, UK. <sup>2</sup>Department of Photonics Engineering, Technical University of Denmark, 2800 Kgs. Lyngby, Denmark. <sup>3</sup>EPSRC National Epitaxy Facility, University of Sheffield, Broad Lane, Sheffield S3 7HQ, UK. <sup>4</sup>Université Côte d'Azur, CNRS, CRHEA, rue Bernard Gregory, 06560 Valbonne, France.

\*These authors contributed equally to this work.

†Corresponding author. Email: dag50@cam.ac.uk (D.A.G.); ma424@cam.ac.uk (M.A.)

‡Present address: Anyon Systems, 1985 55e Avenue #100, Dorval, QC H9P 1G9, Canada.

**Coherent excitation of an ensemble of quantum objects underpins quantum many-body phenomena and offers the opportunity to realize a memory that stores quantum information. Thus far, a deterministic and coherent interface between a spin qubit and such an ensemble has remained elusive. Here, we first use an electron to cool the mesoscopic nuclear-spin ensemble of a semiconductor quantum dot to the nuclear sideband-resolved regime. We then implement an all-optical approach to access individual quantized electronic-nuclear spin transitions. Finally, we perform coherent optical rotations of a single collective nuclear spin excitation—a spin wave. These results constitute the building blocks of a dedicated local memory per quantum-dot spin qubit and promise a solid-state platform for quantum-state engineering of isolated many-body systems.**

A controllable quantum system provides a versatile interface to observe and manipulate the quantum properties of an isolated many-body system (1). In turn, collective excitations of this ensemble can store quantum information as a memory (2, 3)—a contemporary challenge for quantum technologies. While a number of hybrid qubit-ensemble approaches have been pursued in the last decade (4, 5), nuclear spins remain the most promising ensemble candidate owing to their unparalleled coherence times. Such a nuclear ensemble interfaced with a (spin) qubit is described elegantly by the central spin model (6, 7), studied in donor atoms embedded in Si (8, 9), diamond color centers (10–12), and semiconductor nanostructures (13–16). In these systems, the state of the central spin and of the spin ensemble that surrounds it are tied by mutual interaction, allowing proxy control over the many-body system and long-lived storage in principle (2). Realizing this scenario with an electron in a semiconductor quantum dot (QD) offers access to a large ensemble of nuclear spins with quasi-uniform coupling to the central spin. In this system, coherent addressing of the ensemble via the central spin has yet to be shown, and a limiting factor is the thermal fluctuations of the surrounding spins that obfuscate the state-selective transitions required for such control. However, driving the central spin can stimulate exchange of energy with its surrounding spins, and thus modify the properties of its own environment. This has been shown to reduce the uncertainty on the collective spin state of the isolated QD nuclei, leading to prolonged electron spin coherence (17–21).

In this Report, we use all-optical stimulated Raman transitions to manipulate the electron-nuclear system and realize a coherent interface. First employing a configuration analogous to Raman cooling of atoms (22), we drive the electron spin to reduce the thermal fluctuations of the nuclear spin ensemble (Fig. 1A). Cooling the nuclear spin fluctuations to an effective temperature well below the nuclear Zeeman energy (<1 mK), followed immediately by detuned probing of the electron spin resonance (ESR), we reveal an excitation spectrum of transitions between many-body states that are collectively enhanced by the creation of a single nuclear spin-wave excitation—a nuclear magnon. Finally, we drive a single magnon transition resonantly, inducing coherent exchange between the electron spin and the nuclear spin ensemble.

Our system consists of a charge-controlled semiconductor QD (23), where a single electron spin is coupled optically to a charged exciton state, and magnetically to an isolated reservoir of  $N$  ( $10^4$  to  $10^5$ ) nuclear spins of As (total spin  $I = 3/2$ ), Ga ( $I = 3/2$ ), and In ( $I = 3/2$ ), as in Fig. 1B. We drive the electron-nuclear system with a narrow two-photon resonance at detuning  $\delta$  from an excited state, whose linewidth  $\Gamma$  is tunable via the optical pumping rate of the electron spin (Fig. 1B), as with Raman cooling (22). The optical parameters set the dissipation rate relative to the energy scales relevant for cooling, which are the nuclear Zeeman energy  $\omega_n$  and the hyperfine coupling energy per nucleus  $A_n$ , like the phonon and photon recoil energies for trapped atoms (22). In atomic physics, the motion of an atom relative to detuned driving fields leads to a velocity-dependent absorption rate via the

Doppler effect and, together with the photon recoil momentum, to a damping force that is the basis of laser cooling of atomic motion (24). In our system, the hyperfine interaction between the electron and nuclei leads to a shift of the ESR that depends linearly on the net polarization  $I_z$  of the nuclei (6); this Overhauser shift  $2A_c I_z$  thus leads to a polarization-dependent absorption rate. In the presence of material strain, the hyperfine interaction enables optically driven nuclear spin flips that can be modeled as sidebands of amplitude  $\eta\Omega$  ( $\eta < 1$ ) on a principal transition of amplitude  $\Omega$  that flips the electron spin only (25, 26). With fast electron spin reset, absorption on the sidebands at polarization-dependent rates  $W_{\pm}(I_z)$  can increase (+) or decrease (−) the mean nuclear polarization  $I_z$ , as shown in Fig. 1C, in a process known as dynamic nuclear polarization (6, 27). The evolution of this complex system pitting drift  $W_{\pm}$  against diffusion  $\Gamma_d(I_z)$  is captured elegantly by a simple rate equation (26, 28):

$$\frac{dI_z}{dt} = -\frac{\Gamma_{\text{tot}}}{(3N/2)} [I_z - f(I_z)] \quad (1)$$

where  $\Gamma_{\text{tot}} = W_+ + W_- + \Gamma_d$  is the total diffusion rate and  $f(I_z) = (3N/2)(W_+ + W_-)/\Gamma_{\text{tot}}$  is the cooling function that reduces fluctuations, as in Doppler cooling (24). The polarization  $I_0 = \delta/(2A_c)$  is the steady-state of the dynamical system defined by Eq. 1, as shown in Fig. 1C. Rate extrema occur when the Overhauser shift brings a sideband transition in resonance with the drive,  $|2A_c(I_z - I_0)| \approx \omega_n$  (for  $\omega_n \gg A_c$ ), suggesting that Overhauser fluctuations can be reduced below the nuclear Zeeman energy,  $\omega_n$ . The driven ensemble experiences damping proportional to the cooling-function gradient,  $(5/3)f'(I_0)$ . For a probability distribution  $p(I_z)$ , the fluctuations  $\Delta I_z^2$  are reduced from their thermal-equilibrium value  $5N/4$  (Fig. 1C) by (23, 28)

$$\frac{\Delta I_z^2}{5N/4} = \frac{1 - \left(\frac{2}{5N} I_0\right)^2}{1 - \frac{5}{3} f'(I_0)} \quad (2)$$

From the electron's perspective, a commensurate reduction of fluctuations occurs for a highly polarized nuclear ensemble, which to-date has not been achieved. This occurs at thermal equilibrium when the energy  $k_B T$  falls below the system's defining energy scale, here the nuclear Zeeman energy  $\hbar\omega_n$ . The fluctuations in Fig. 1C thus correspond to an effective temperature below  $T = \hbar\omega_n / k_B = 1 \text{ mK}$  (23).

Figure 2 highlights the optimal conditions for cooling the nuclear ensemble. The electron coherence time  $T_2^*$  is a direct measure of nuclear polarization fluctuations  $\Delta I_z^2 = 1/2(A_c T_2^*)^2$  (21, 23), therefore Ramsey interferometry on the electron spin (29, 30) serves as our thermometer. We parametrize temperature as a cooling performance factor

$(5N/4)/\Delta I_z^2$  as a function of Raman rate  $\Omega$  and excited-state linewidth  $\Gamma$ , as shown in Fig. 2A. A maximum of  $\sim 300$  is found where the Raman rate  $\Omega = 17 \text{ MHz}$  is approximately half of the nuclear Zeeman splitting  $\omega_n = 36 \text{ MHz}$ , and the excited-state linewidth corresponds to optical saturation,  $\Gamma \sim 25 \text{ MHz}$ . This is in quantitative agreement with our theoretical prediction, shown in Fig. 2B, that accounts for nuclear-spin diffusion and inhomogeneous broadening (23).

The Raman rate  $\Omega$  and the electronic excited-state linewidth  $\Gamma$  determine the spectral selectivity and the diffusion rate of the cooling process. For best cooling, no absorption should occur at the stable point  $I_0$ , while sideband absorption should turn on sharply in response to polarization fluctuations away from  $I_0$ . Optimal values for  $\Omega$  and  $\Gamma$  thus depend on the sideband spacing  $\omega_n$ :  $\Omega, \Gamma \ll \omega_n$  entails high spectral selectivity but weak sideband absorption near  $I_0$ , while  $\Omega, \Gamma \sim \omega_n$  entails strong absorption on the sidebands but low spectral selectivity. Figure 2C depicts this dependence of the cooling function  $f(I_z)$  on the optical parameters: the damping  $f'(I_0)$  is largest when the Raman rate is approximately half of the nuclear Zeeman energy,  $\Omega \sim \omega_n/2$ , and when close to saturation  $\Omega \sim \Gamma/\sqrt{2}$ . We confirm this experimentally in Fig. 2D by changing the applied magnetic field: the values of  $\Omega$  and  $\Gamma$  that optimize the cooling performance are proportional to the sideband spacing.

The lowest temperature of our system is a function of distinct diffusion and broadening processes competing with Raman cooling, through magnetic-field dependent rates: in the low-field regime, homogeneous broadening of the ESR dominates (29, 30) (purple region in Fig. 2E), while in the high-field regime optical diffusion does (23) (red region in Fig. 2E). Further, electron-mediated nuclear spin diffusion (31, 32) counteracts Raman cooling in both regimes. Figure 2E displays the magnetic field dependence of the temperature optimized against optical parameters. Our results follow closely the field-dependent bounds obtained from modelling the diffusion processes (solid curve), and establish the globally optimal cooling performance of  $\sim 400$  at  $\sim 3.3 \text{ T}$ . Operating close to this field, we prepare the nuclear ensemble at an effective temperature of  $200 \text{ } \mu\text{K}$  (23). There, the Overhauser fluctuations are well below the nuclear Zeeman splitting,  $2A_c \sqrt{\Delta I_z^2} = 7 \text{ MHz} < \omega_n = 22 \text{ MHz}$  (at  $3 \text{ T}$ ), which places our system well into the sideband-resolved regime.

We now probe the electron-spin state in the coherent regime where dissipation is turned off,  $\Gamma \rightarrow 0$ . We drive the ESR for a time  $\tau$  at a detuning  $\delta$  and measure the electron  $|\downarrow\rangle$  population (Fig. 3A). Figure 3B shows this time-resolved spectrum obtained from our theoretical analysis (23), where we expect five distinct processes, as shown in Fig. 3C: a central transition at  $\delta = 0$ , and four sideband transitions at  $\delta = \pm\omega_n$ ,

$\pm 2\omega_n$ . The nuclear spin-flip transitions originate from the strain-induced electric field gradient that couples to the quadrupole moment of all QD nuclei, mixing their Zeeman eigenstates (16). The quadratic nature of this interaction allows the nuclear polarization to change either by one quantum ( $I_z \rightarrow I_z \pm 1$ ) (25, 26) or by two quanta ( $I_z \rightarrow I_z \pm 2$ ); these selection rules apply to all QD nuclear spin species. A first-order perturbative expansion of the hyperfine interaction (23) dresses the ESR with these transitions. When the driving field with amplitude  $\Omega$  is detuned from the principal transition by one or two units of nuclear Zeeman energy  $\omega_n$ , these resonant transitions occur with an amplitude  $\eta\Omega$ , as sidebands of strength  $\eta = \mathcal{D}A_{nc} / \omega_n$ ; here  $A_{nc} \approx 0.015A_c$  is the non-collinear hyperfine constant parametrizing the perturbation. The driven electron cannot distinguish the  $\sim N$  possible spin-flips that take  $I_z$  to  $I_z \pm 1, \pm 2$ , which leads to the degeneracy factor  $\mathcal{D} \sim \sqrt{N}$ . This underpins the collective enhancement (33) that makes the nuclear spin-flip sideband transitions so prominent in our system.

Figure 3D shows the experimental spectra averaged over short delays  $\tau = 0 - 150$  ns, where  $\Omega\tau \sim \pi$ , revealing the principal ESR with optimal (violet data) and suboptimal (red data) cooling. The feature width is a convolution of the drive Rabi frequency  $\Omega$  with the Overhauser field fluctuations  $2A_c\sqrt{\Delta I_z^2}$ , and highlights the spectral narrowing achieved by Raman cooling. Figure 3E shows the time-frequency map of this measurement. At  $\delta = 0$ , the principal ESR leads to Rabi oscillations at  $\Omega = 3.8$  MHz. At larger delays where  $\eta\Omega\tau \sim \pi$  and at a sufficient detuning from the principal transition  $\delta \gg \Omega$ , the emergence of four sideband processes agrees well with our predictions. Figure 3F is a standout observation of the sideband spectrum, integrated over  $\tau = 850 - 1000$  ns. A five-Gaussian fit (dashed curve) verifies that the sidebands emerge at integer multiples of  $\omega_n$ , and the shaded area highlights the theoretical spectrum. Our results confirm that the sideband drive can excite selectively a single nuclear spin-flip in the ensemble and highlight that  $\sim N$  sufficiently identical nuclei are simultaneously coupled to the driven electron. In contrast to magnons in ferromagnetic materials, this type of collective excitation is based on an electron-mediated interaction, in close analogy to photon-mediated magnon-polariton modes in strongly coupled light-matter interfaces (3). Until now, such a collective nuclear-spin excitation had only been observed as ensemble measurements of atomic gases (34) and magnetic materials (35, 36), while our result represents the deterministic generation of a single nuclear magnon by interfacing the nuclei with an elementary controllable quantum system.

This spectral selectivity enables coherent generation of a single-spin excitation, provided it is faster than the dephasing times of the electron ( $T_2 \approx 1$   $\mu$ s) (30) and the nuclei ( $T_2 \approx 10$

$\mu$ s) (32). Figure 4 illustrates this coherent drive via Rabi oscillations. Detuning maximally from the quenching effect of coupling to the principal transition, we drive one of the second sidebands ( $I_z \rightarrow I_z + 2$ ) with  $\eta\Omega > 1/T_2$  (Fig. 3C), and measure for delays  $\tau \gtrsim \pi / \eta\Omega$ . Figure 4 presents measurements with three Rabi frequencies  $\Omega = 7, 9, 12$  MHz (23). Oscillations of the electron spin population at a fraction  $\eta$  of the carrier frequency  $\Omega$  are a direct measurement of coherent electron-nuclear dynamics. We attribute the sharp appearance of oscillations above a Rabi frequency  $\Omega \sim 10$  MHz to reaching a sufficient sideband coupling  $\eta\Omega \sim 1.5$  MHz to overcome inhomogeneities, which exist on a MHz-scale within a more strongly coupled subset of nuclei (23). Our master equation model (solid lines in Fig. 4) captures this inhomogeneous broadening that limits the Rabi oscillations. The gray-shaded areas represent  $\pm 20\%$  deviations of Rabi frequency, and our data's drift toward lower Rabi frequency at long delays suggests a dephasing mechanism that depends on accumulated phase  $\Omega\tau$ . Our model further allows us to reconstruct the nuclear-spin population transfer, where the effect of off-resonant excitation of the principal transition is not present, and shows that the electron spin population transfer is accompanied predominantly by nuclear spin population transfer (23).

The value  $\eta \sim 15\%$ , directly extracted from the coherent oscillations in Fig. 4, confirms the  $\sim \sqrt{N}$  enhancement of the sideband transition strength arising from the collective nature of the magnon excitation. Indeed, owing to sufficient coupling homogeneity, the nuclei can be treated as an ensemble of  $N = 30,000$  indistinguishable spins under the hyperfine interaction with the electron. Oscillations in Fig. 4 indicate the creation and retrieval of a coherent superposition of a single nuclear spin excitation among all spins, forming the basis of many-body entanglement as found for Dicke states (33). This occurs despite operating near zero polarization, where the degeneracy of nuclear states is maximal. Strikingly, this exchange of coherence is far from the bosonic approximation available for a fully polarized ensemble (2). Furthermore, an intermediate drive time  $\eta\Omega\tau = \pi/2$  generates an inseparable coherent superposition state for the electron and the nuclei.

In this work, we have realized a coherent quantum interface between a single electron and 30,000 nuclei using light. Making use of the back-action of a single nuclear-spin flip on the electron, the development of a dedicated quantum memory per electron spin qubit in semiconductor QDs becomes viable. Future possibilities also include creating and monitoring tailored collective quantum states of the nuclear ensemble, such as Schrödinger cat states, by harnessing Hamiltonian engineering techniques.

## REFERENCES AND NOTES

1. L. Amico, R. Fazio, A. Osterloh, V. Vedral, Entanglement in many-body systems. *Rev. Mod. Phys.* **80**, 517–576 (2008). doi:10.1103/RevModPhys.80.517



2. J. M. Taylor, C. M. Marcus, M. D. Lukin, Long-lived memory for mesoscopic quantum bits. *Phys. Rev. Lett.* **90**, 206803 (2003). [doi:10.1103/PhysRevLett.90.206803](https://doi.org/10.1103/PhysRevLett.90.206803) [Medline](#)
3. K. S. Choi, A. Goban, S. B. Papp, S. J. van Enk, H. J. Kimble, Entanglement of spin waves among four quantum memories. *Nature* **468**, 412–416 (2010). [doi:10.1038/nature09568](https://doi.org/10.1038/nature09568) [Medline](#)
4. X. Zhu, S. Saito, A. Kemp, K. Kakuyanagi, S. Karimoto, H. Nakano, W. J. Munro, Y. Tokura, M. S. Everitt, K. Nemoto, M. Kasu, N. Mizuochi, K. Semba, Coherent coupling of a superconducting flux qubit to an electron spin ensemble in diamond. *Nature* **478**, 221–224 (2011). [doi:10.1038/nature10462](https://doi.org/10.1038/nature10462) [Medline](#)
5. Y. Tabuchi, S. Ishino, A. Noguchi, T. Ishikawa, R. Yamazaki, K. Usami, Y. Nakamura, Coherent coupling between a ferromagnetic magnon and a superconducting qubit. *Science* **349**, 405–408 (2015). [doi:10.1126/science.aaa3693](https://doi.org/10.1126/science.aaa3693) [Medline](#)
6. A. Abragam, L. C. Hebel, The principles of nuclear magnetism. *Am. J. Phys.* **29**, 860–861 (1961). [doi:10.1119/1.1937646](https://doi.org/10.1119/1.1937646)
7. D. Stanek, C. Raas, G. S. Uhrig, From quantum-mechanical to classical dynamics in the central-spin model. *Phys. Rev. B* **90**, 064301 (2014). [doi:10.1103/PhysRevB.90.064301](https://doi.org/10.1103/PhysRevB.90.064301)
8. R. de Sousa, S. Das Sarma, Theory of nuclear-induced spectral diffusion: Spin decoherence of phosphorus donors in Si and GaAs quantum dots. *Phys. Rev. B* **68**, 115322 (2003). [doi:10.1103/PhysRevB.68.115322](https://doi.org/10.1103/PhysRevB.68.115322)
9. J. J. Pla, K. Y. Tan, J. P. Dehollain, W. H. Lim, J. J. L. Morton, D. N. Jamieson, A. S. Dzurak, A. Morello, A single-atom electron spin qubit in silicon. *Nature* **489**, 541–545 (2012). [doi:10.1038/nature11449](https://doi.org/10.1038/nature11449) [Medline](#)
10. L. Childress, M. V. Gurudev Dutt, J. M. Taylor, A. S. Zibrov, F. Jelezko, J. Wrachtrup, P. R. Hemmer, M. D. Lukin, Coherent dynamics of coupled electron and nuclear spin qubits in diamond. *Science* **314**, 281–285 (2006). [doi:10.1126/science.1131871](https://doi.org/10.1126/science.1131871) [Medline](#)
11. G. Balasubramanian, P. Neumann, D. Twitchen, M. Markham, R. Kolesov, N. Mizuochi, J. Isoya, J. Achard, J. Beck, J. Tisler, V. Jacques, P. R. Hemmer, F. Jelezko, J. Wrachtrup, Ultralong spin coherence time in isotopically engineered diamond. *Nat. Mater.* **8**, 383–387 (2009). [doi:10.1038/nmat2420](https://doi.org/10.1038/nmat2420) [Medline](#)
12. N. Kalb, A. A. Reiserer, P. C. Humphreys, J. J. W. Bakermans, S. J. Kamerling, N. H. Nickerson, S. C. Benjamin, D. J. Twitchen, M. Markham, R. Hanson, Entanglement distillation between solid-state quantum network nodes. *Science* **356**, 928–932 (2017). [doi:10.1126/science.aan0070](https://doi.org/10.1126/science.aan0070) [Medline](#)
13. A. V. Khaetskii, D. Loss, L. Glazman, Electron spin decoherence in quantum dots due to interaction with nuclei. *Phys. Rev. Lett.* **88**, 186802 (2002). [doi:10.1103/PhysRevLett.88.186802](https://doi.org/10.1103/PhysRevLett.88.186802) [Medline](#)
14. I. A. Merkulov, A. L. Efros, M. Rosen, Electron spin relaxation by nuclei in semiconductor quantum dots. *Phys. Rev. B* **65**, 205309 (2002). [doi:10.1103/PhysRevB.65.205309](https://doi.org/10.1103/PhysRevB.65.205309)
15. H. Bluhm, S. Foletti, I. Neder, M. Rudner, D. Mahalu, V. Umansky, A. Yacoby, Dephasing time of GaAs electron-spin qubits coupled to a nuclear bath exceeding 200  $\mu$ s. *Nat. Phys.* **7**, 109–113 (2011). [doi:10.1038/nphys1856](https://doi.org/10.1038/nphys1856)
16. B. Urbaszek, X. Marie, T. Amand, O. Krebs, P. Voisin, P. Maletinsky, A. Högele, A. Imamoglu, Nuclear spin physics in quantum dots: An optical investigation. *Rev. Mod. Phys.* **85**, 79–133 (2013). [doi:10.1103/RevModPhys.85.79](https://doi.org/10.1103/RevModPhys.85.79)
17. D. Stepanenko, G. Burkard, G. Giedke, A. Imamoglu, Enhancement of electron spin coherence by optical preparation of nuclear spins. *Phys. Rev. Lett.* **96**, 136401 (2006). [doi:10.1103/PhysRevLett.96.136401](https://doi.org/10.1103/PhysRevLett.96.136401) [Medline](#)
18. A. Greilich, A. Shabae, D. R. Yakovlev, A. L. Efros, I. A. Yugova, D. Reuter, A. D. Wieck, M. Bayer, Nuclei-induced frequency focusing of electron spin coherence. *Science* **317**, 1896–1899 (2007). [doi:10.1126/science.1146850](https://doi.org/10.1126/science.1146850) [Medline](#)
19. D. J. Reilly, J. M. Taylor, J. R. Petta, C. M. Marcus, M. P. Hanson, A. C. Gossard, Suppressing spin qubit dephasing by nuclear state preparation. *Science* **321**, 817–821 (2008). [doi:10.1126/science.1159221](https://doi.org/10.1126/science.1159221) [Medline](#)
20. X. Xu, W. Yao, B. Sun, D. G. Steel, A. S. Bracker, D. Gammon, L. J. Sham, Optically controlled locking of the nuclear field via coherent dark-state spectroscopy. *Nature* **459**, 1105–1109 (2009). [doi:10.1038/nature08120](https://doi.org/10.1038/nature08120) [Medline](#)
21. G. Éthier-Majcher, D. Gangloff, R. Stockill, E. Clarke, M. Hugues, C. Le Gall, M. Atatüre, Improving a solid-state qubit through an engineered mesoscopic environment. *Phys. Rev. Lett.* **119**, 130503 (2017). [doi:10.1103/PhysRevLett.119.130503](https://doi.org/10.1103/PhysRevLett.119.130503) [Medline](#)
22. D. J. Heinzen, D. J. Wineland, Quantum-limited cooling and detection of radio-frequency oscillations by laser-cooled ions. *Phys. Rev. A* **42**, 2977–2994 (1990). [doi:10.1103/PhysRevA.42.2977](https://doi.org/10.1103/PhysRevA.42.2977) [Medline](#)
23. Supplementary materials.
24. W. D. Phillips, Nobel Lecture: Laser cooling and trapping of neutral atoms. *Rev. Mod. Phys.* **70**, 721–741 (1998). [doi:10.1103/RevModPhys.70.721](https://doi.org/10.1103/RevModPhys.70.721)
25. C.-W. Huang, X. Hu, Theoretical study of nuclear spin polarization and depolarization in self-assembled quantum dots. *Phys. Rev. B* **81**, 205304 (2010). [doi:10.1103/PhysRevB.81.205304](https://doi.org/10.1103/PhysRevB.81.205304)
26. A. Högele, M. Kroner, C. Latta, M. Claassen, I. Carusotto, C. Bulutay, A. Imamoglu, Dynamic nuclear spin polarization in the resonant laser excitation of an InGaAs quantum dot. *Phys. Rev. Lett.* **108**, 197403 (2012). [doi:10.1103/PhysRevLett.108.197403](https://doi.org/10.1103/PhysRevLett.108.197403) [Medline](#)
27. B. Eble, O. Krebs, A. Lemaître, K. Kowalik, A. Kudelski, P. Voisin, B. Urbaszek, X. Marie, T. Amand, Dynamic nuclear polarization of a single charge-tunable InAs / GaAs quantum dot. *Phys. Rev. B* **74**, 081306 (2006). [doi:10.1103/PhysRevB.74.081306](https://doi.org/10.1103/PhysRevB.74.081306)
28. W. Yang, L. J. Sham, General theory of feedback control of a nuclear spin ensemble in quantum dots. *Phys. Rev. B* **88**, 235304 (2013). [doi:10.1103/PhysRevB.88.235304](https://doi.org/10.1103/PhysRevB.88.235304)
29. A. Bechtold, D. Rauch, F. Li, T. Simmet, P.-L. Audebert, A. Regler, K. Müller, N. A. Sinitsyn, J. J. Finley, Three-stage decoherence dynamics of an electron spin qubit in an optically active quantum dot. *Nat. Phys.* **11**, 1005–1008 (2015). [doi:10.1038/nphys3470](https://doi.org/10.1038/nphys3470)
30. R. Stockill, C. Le Gall, C. Matthiesen, L. Huthmacher, E. Clarke, M. Hugues, M. Atatüre, Quantum dot spin coherence governed by a strained nuclear environment. *Nat. Commun.* **7**, 12745 (2016). [doi:10.1038/ncomms12745](https://doi.org/10.1038/ncomms12745) [Medline](#)
31. C. Latta, A. Srivastava, A. Imamoglu, Hyperfine interaction-dominated dynamics of nuclear spins in self-assembled InGaAs quantum dots. *Phys. Rev. Lett.* **107**, 167401 (2011). [doi:10.1103/PhysRevLett.107.167401](https://doi.org/10.1103/PhysRevLett.107.167401) [Medline](#)
32. G. Wüst, M. Munsch, F. Maier, A. V. Kuhlmann, A. Ludwig, A. D. Wieck, D. Loss, M. Poggio, R. J. Warburton, Role of the electron spin in determining the coherence of the nuclear spins in a quantum dot. *Nat. Nanotechnol.* **11**, 885–889 (2016). [doi:10.1038/nnano.2016.114](https://doi.org/10.1038/nnano.2016.114) [Medline](#)
33. R. H. Dicke, Coherence in spontaneous radiation processes. *Phys. Rev.* **93**, 99–110 (1954). [doi:10.1103/PhysRev.93.99](https://doi.org/10.1103/PhysRev.93.99)
34. B. R. Johnson, J. S. Denker, N. Bigelow, L. P. Lévy, J. H. Freed, D. M. Lee, Observation of nuclear spin waves in spin-polarized atomic hydrogen gas. *Phys. Rev. Lett.* **52**, 1508–1511 (1984). [doi:10.1103/PhysRevLett.52.1508](https://doi.org/10.1103/PhysRevLett.52.1508)
35. G. Seewald, E. Hagn, E. Zech, Observation of a nuclear-magnon contribution to the nuclear spin-lattice relaxation of  $^{191}\text{Pt}$  in ferromagnetic cobalt. *Phys. Rev. Lett.* **78**, 5002–5005 (1997). [doi:10.1103/PhysRevLett.78.5002](https://doi.org/10.1103/PhysRevLett.78.5002)
36. L. V. Abdurakhimov, Y. M. Bunkov, D. Konstantinov, Normal-mode splitting in the coupled system of hybridized nuclear magnons and microwave photons. *Phys. Rev. Lett.* **114**, 226402 (2015). [doi:10.1103/PhysRevLett.114.226402](https://doi.org/10.1103/PhysRevLett.114.226402) [Medline](#)
37. D. Press, T. D. Ladd, B. Zhang, Y. Yamamoto, Complete quantum control of a single quantum dot spin using ultrafast optical pulses. *Nature* **456**, 218–221 (2008). [doi:10.1038/nature07530](https://doi.org/10.1038/nature07530) [Medline](#)
38. A. Greilich, S. E. Economou, S. Spatzek, D. R. Yakovlev, D. Reuter, A. D. Wieck, T. L. Reinecke, M. Bayer, Ultrafast optical rotations of electron spins in quantum dots. *Nat. Phys.* **5**, 262–266 (2009). [doi:10.1038/nphys1226](https://doi.org/10.1038/nphys1226)
39. A. R. Onur, C. H. van der Wal, Two-laser dynamic nuclear polarization with semiconductor electrons: Feedback, suppressed fluctuations, and bistability near two-photon resonance. *Phys. Rev. B* **98**, 165304 (2018). [doi:10.1103/PhysRevB.98.165304](https://doi.org/10.1103/PhysRevB.98.165304)
40. I. T. Vink, K. C. Nowack, F. H. L. Koppens, J. Danon, Y. V. Nazarov, L. M. K. Vandersypen, Locking electron spins into magnetic resonance by electron–nuclear feedback. *Nat. Phys.* **5**, 764–768 (2009). [doi:10.1038/nphys1366](https://doi.org/10.1038/nphys1366)
41. H. Bluhm, S. Foletti, D. Mahalu, V. Umansky, A. Yacoby, Enhancing the coherence of a spin qubit by operating it as a feedback loop that controls its nuclear spin bath. *Phys. Rev. Lett.* **105**, 216803 (2010). [doi:10.1103/PhysRevLett.105.216803](https://doi.org/10.1103/PhysRevLett.105.216803) [Medline](#)

42. M. Issler, E. M. Kessler, G. Giedke, S. Yelin, I. Cirac, M. D. Lukin, A. Imamoglu, Nuclear spin cooling using Overhauser-field selective coherent population trapping. *Phys. Rev. Lett.* **105**, 267202 (2010). [doi:10.1103/PhysRevLett.105.267202](https://doi.org/10.1103/PhysRevLett.105.267202) [Medline](#)
43. C. M. Chow, A. M. Ross, D. Kim, D. Gammon, A. S. Bracker, L. J. Sham, D. G. Steel, Nonlocal nuclear spin quieting in quantum dot molecules: Optically induced extended two-electron spin coherence time. *Phys. Rev. Lett.* **117**, 077403 (2016). [doi:10.1103/PhysRevLett.117.077403](https://doi.org/10.1103/PhysRevLett.117.077403) [Medline](#)
44. D. Press, K. De Greve, P. L. McMahon, T. D. Ladd, B. Friess, C. Schneider, M. Kamp, S. Höfling, A. Forchel, Y. Yamamoto, Ultrafast optical spin echo in a single quantum dot. *Nat. Photonics* **4**, 367–370 (2010). [doi:10.1038/nphoton.2010.83](https://doi.org/10.1038/nphoton.2010.83)
45. C. Bulutay, Quadrupolar spectra of nuclear spins in strained  $\text{In}_x\text{Ga}_{1-x}\text{As}$  quantum dots. *Phys. Rev. B* **85**, 115313 (2012). [doi:10.1103/PhysRevB.85.115313](https://doi.org/10.1103/PhysRevB.85.115313)
46. J. R. Schrieffer, P. A. Wolff, Relation between the Anderson and Kondo Hamiltonians. *Phys. Rev.* **149**, 491–492 (1966). [doi:10.1103/PhysRev.149.491](https://doi.org/10.1103/PhysRev.149.491)
47. S. Bravyi, D. P. DiVincenzo, D. Loss, Schrieffer–Wolff transformation for quantum many-body systems. *Ann. Phys.* **326**, 2793–2826 (2011). [doi:10.1016/j.aop.2011.06.004](https://doi.org/10.1016/j.aop.2011.06.004)
48. B. Urbaszek, P.-F. Braun, T. Amand, O. Krebs, T. Belhadj, A. Lemaître, P. Voisin, X. Marie, Efficient dynamical nuclear polarization in quantum dots: Temperature dependence. *Phys. Rev. B* **76**, 201301 (2007). [doi:10.1103/PhysRevB.76.201301](https://doi.org/10.1103/PhysRevB.76.201301)
49. A. I. Tartakovskii, T. Wright, A. Russell, V. I. Fal'ko, A. B. Van'kov, J. Skiba-Szymanska, I. Drouzas, R. S. Kolodka, M. S. Skolnick, P. W. Fry, A. Tahraoui, H.-Y. Liu, M. Hopkinson, Nuclear spin switch in semiconductor quantum dots. *Phys. Rev. Lett.* **98**, 026806 (2007). [doi:10.1103/PhysRevLett.98.026806](https://doi.org/10.1103/PhysRevLett.98.026806) [Medline](#)
50. P. Maletinsky, A. Badolato, A. Imamoglu, Dynamics of quantum dot nuclear spin polarization controlled by a single electron. *Phys. Rev. Lett.* **99**, 056804 (2007). [doi:10.1103/PhysRevLett.99.056804](https://doi.org/10.1103/PhysRevLett.99.056804) [Medline](#)
51. J. Wesenberg, K. Mølmer, Mixed collective states of many spins. *Phys. Rev. A* **65**, 062304 (2002). [doi:10.1103/PhysRevA.65.062304](https://doi.org/10.1103/PhysRevA.65.062304)

## ACKNOWLEDGMENTS

We thank A. Nunnenkamp and G. Burkard for critical reading of the manuscript and R. Stockill for helpful discussions. **Funding:** This work was supported by ERC PHOENICS (617985) and EPSRC NQIT (EP/M013243/1). Sample growth was carried out in the EPSRC National Epitaxy Facility. D.A.G. acknowledges a St. John's College fellowship, G.E.-M. an NSERC postdoctoral fellowship, E.V.D. the Danish Council for Independent Research (DFF-4181-00416), and C.L.G. a Royal Society fellowship. **Author contributions:** D.A.G., G.E.-M., C.L.G., and M.A. conceived the experiments. D.A.G., G.E.-M., C.L.G., and D.M.J. acquired and analyzed data. D.A.G., G.E.-M., and E.V.D. performed the theory and simulations. E.C. and M.H. grew the sample. D.A.G., G.E.-M., E.V.D., J.H.B., D.M.J., C.L.G., and M.A. prepared the manuscript. **Competing interests:** None declared. **Data and materials availability:** All data needed to evaluate the conclusions in the paper are present in the paper or the supplementary materials.

## SUPPLEMENTARY MATERIALS

[www.sciencemag.org/cgi/content/full/science.aaw2906/DC1](http://www.sciencemag.org/cgi/content/full/science.aaw2906/DC1)  
 Supplementary Text  
 Figs. S1 to S8  
 Tables S1 and S2  
 References (37–51)

6 December 2018; accepted 8 February 2019  
 Published online 21 February 2019  
[10.1126/science.aaw2906](https://doi.org/10.1126/science.aaw2906)

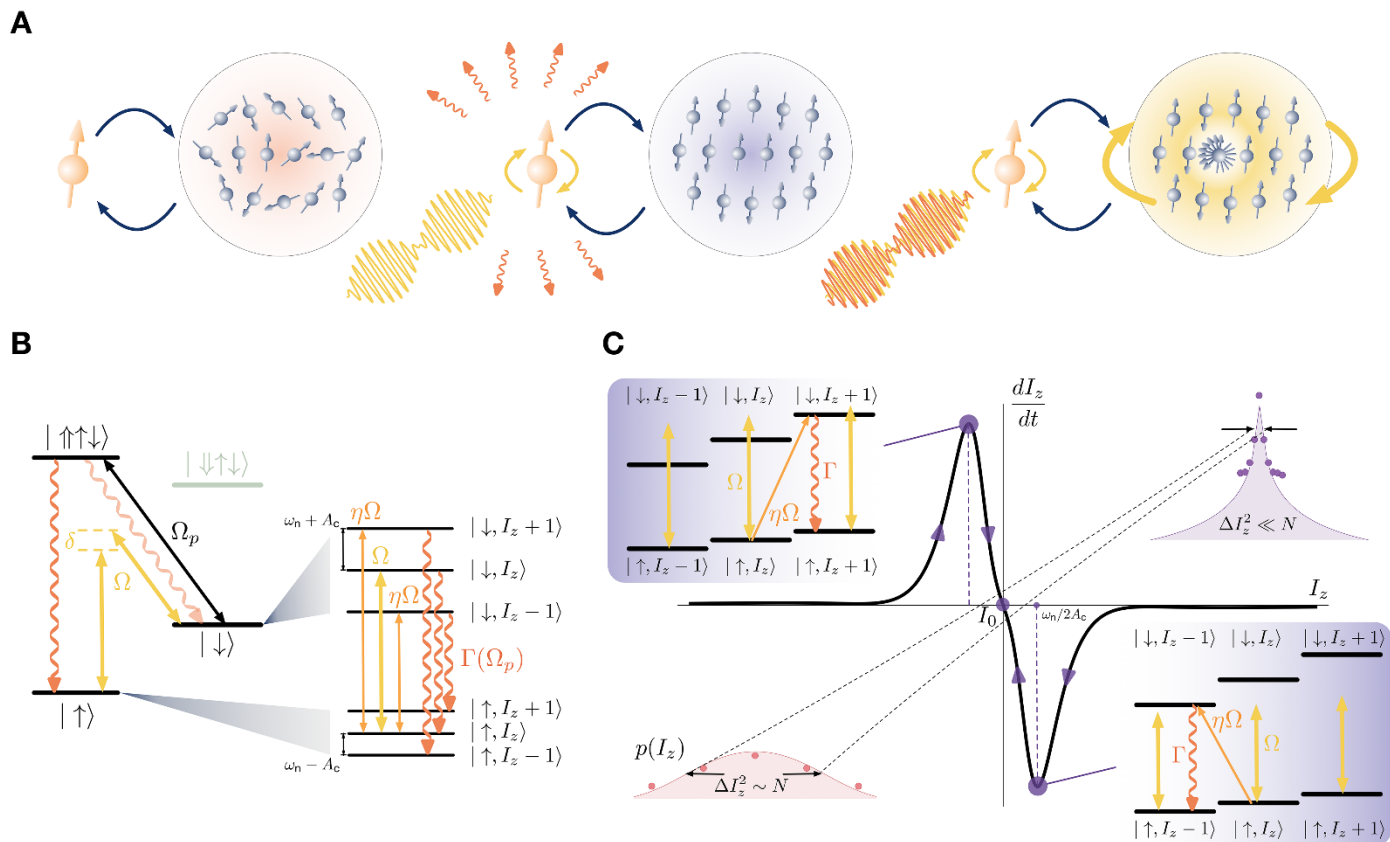


**Fig. 1. An electron controls a nuclear ensemble.** (A) The central spin scenario: (left) a spin interacts with a thermally fluctuating ensemble; (middle) in the presence of dissipation, the driven spin can cool the ensemble to a lower effective temperature; (right) driving the spin can create coherent superpositions of single spin-flips as collective excitations of the cooled ensemble. (B) Realization of this scenario in a semiconductor QD, under a magnetic field in Voigt geometry, optically pumped to electronic spin state  $|\uparrow\rangle$  by a resonant drive  $\Omega_p$  via the trion state  $|\uparrow\uparrow\downarrow\rangle$  of homogeneous linewidth  $\Gamma_0 = 150$  MHz at a rate  $\Gamma \sim \Omega_p^2 / \Gamma_0 \leq 38$  MHz. The electron-spin splitting is (Overhauser) shifted by its hyperfine interaction  $2A_c I_z$ , where  $A_c = 600$  kHz, with an ensemble of  $N$  ( $10^4$  to  $10^5$ ) nuclear spins, described by mean polarization states  $I_z = [-3N/2, 3N/2]$  (taken for spin-3/2). Far-detuned ( $\gtrsim 1$  nm) Raman beams drive the electron spin resonance (ESR) at a Rabi frequency  $\Omega \lesssim 40$  MHz, including transitions that simultaneously flip a single nuclear spin  $I_z \rightarrow I_z \pm 1$  at frequency  $\eta\Omega$  ( $\eta < 1$ ). (C) Cooling dynamics: the time-derivative of polarization  $dI_z/dt$  depends on the polarization  $I_z$ , through the Overhauser shift and the nuclear-spin flipping transitions  $W_{\pm}$ . The polarization  $I_0$  is the dynamical system's stable point, where the width  $\Delta I_z^2$  of the probability distribution  $p(I_z)$  is reduced (violet) compared to its value without cooling (red).

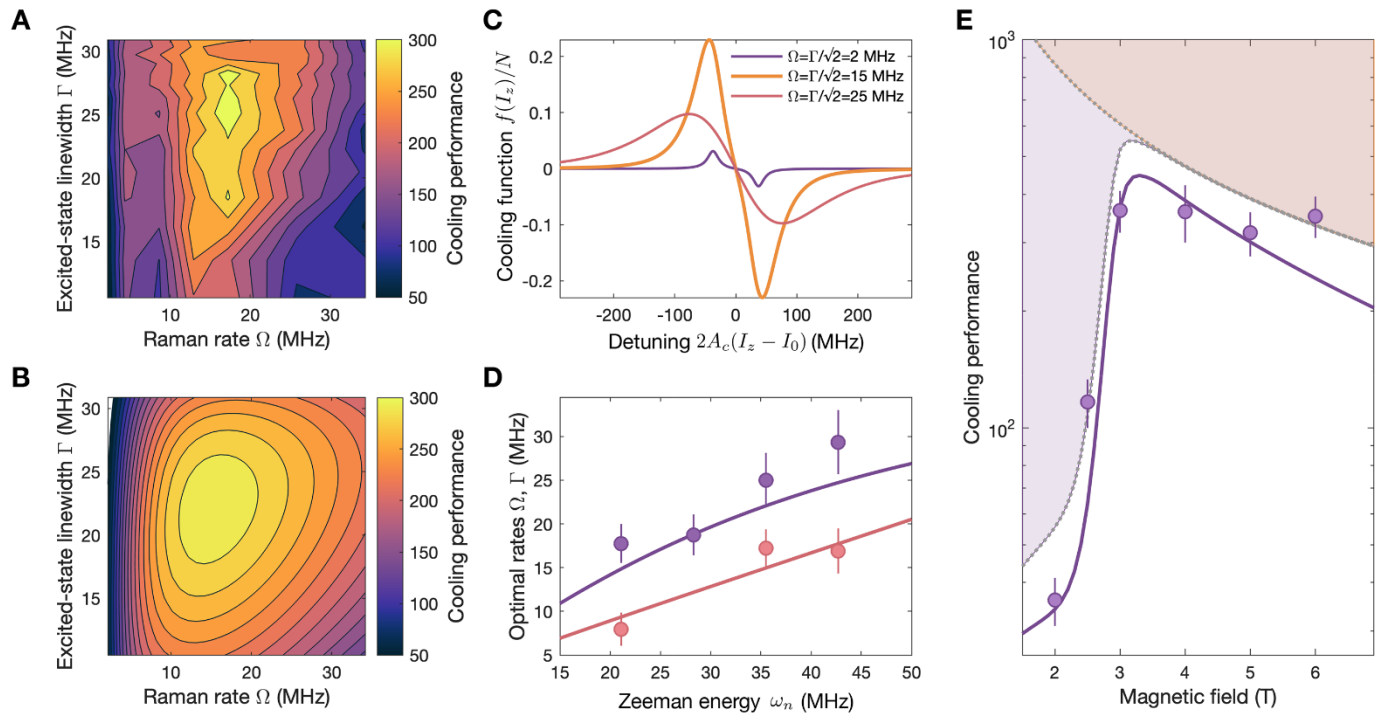


**Fig. 2. Optimal cooling of the nuclear ensemble.** (A) Experimental Raman cooling performance  $5N / 4\Delta I_z^2$  as a function of Raman rate  $\Omega$  and excited-state linewidth  $\Gamma$ , at 5 T. The maximum of 300 is reached for  $\Omega \sim \omega_n/2$ , and saturation conditions  $\Gamma \sim \sqrt{2}\Omega$ . (B) Theoretical prediction of (A). (C) Calculated cooling curves  $f(I_z) \propto W_+ - W_-$  at optical saturation  $\Omega = \Gamma/\sqrt{2}$  for increasing rates. The largest damping  $f'(I_0)$  occurs when  $\Omega \sim \omega_n/2 = 18$  MHz (orange curve). (D) Raman rate and excited-state linewidth at the measured optimal cooling performance as a function of  $\omega_n$  at 3 T, 4 T, 5 T, and 6 T. Solid curves are the corresponding theoretical calculations. (E) Magnetic-field optimal cooling. Circles represent the maximum cooling performance at a given magnetic field. Shaded regions are cooling limits, and curves from a theoretical model [see main text and (23)]. Error bars represent one standard deviation of uncertainty.



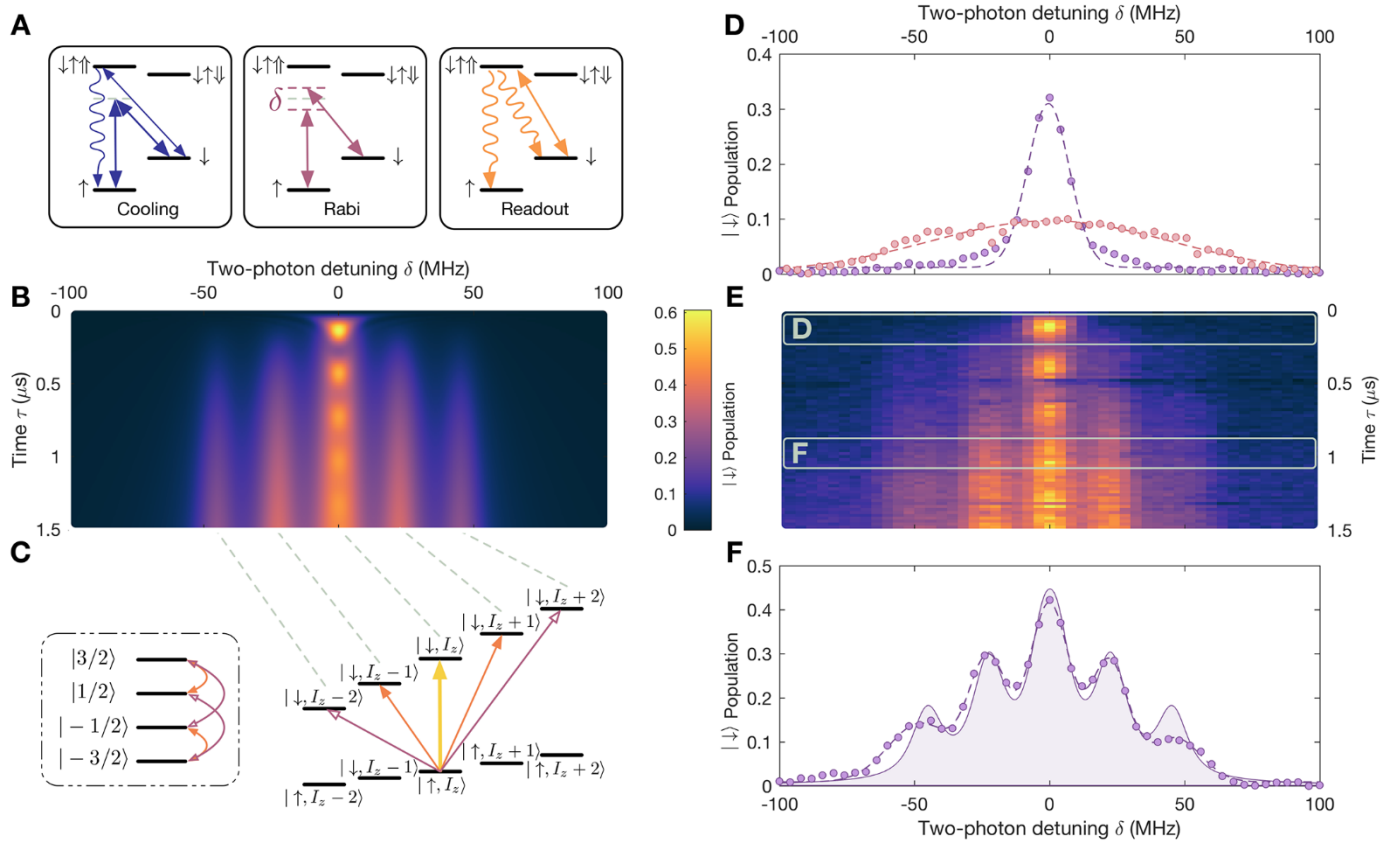


**Fig. 3. Resolving single nuclear magnons.** (A) Spectrum measurement sequence, from left to right: Raman cooling, Rabi drive ESR at detuning  $\delta$  for time  $\tau$ , and optical readout of the electron  $|\downarrow\rangle$  population (23). (B) Theoretical ESR spectrum buildup as a function of two-photon detuning  $\delta$  and drive time  $\tau$ , for a Rabi frequency of  $\Omega = 3.3$  MHz on the central transition. Sideband coupling  $\eta$  is fitted (23). The model is a master equation treatment of the driven electron-nuclear system, accounting for electron dephasing, where the nuclear system is reduced to collective states with polarization close to  $I_0$  (23). (C) On the right, the ladder of electronic and nuclear states showing the carrier  $I_z \rightarrow I_z$  and sideband transitions  $I_z \rightarrow I_z \pm 1, I_z \pm 2$  from an initially spin-up polarized electron at a nuclear polarization of  $I_z$ . On the left, the same transitions represented within a single nuclear spin-3/2 manifold. (D) Spectra with optimal (violet) and poor (red) Raman cooling at average delay  $\tau = 0 - 150$  ns. The dashed curves are Gaussian fits with standard deviation 7.7 MHz and 44.6 MHz, respectively. (E) Experimental spectrum buildup with  $\Omega = 3.8$  MHz. (F) Spectrum at integrated delay  $\tau = 850 - 1000$  ns. The solid curve is the same time slice averaged from the theory spectrum of (B). The dashed curve is five Gaussian functions centered at  $\delta \sim 0, \pm\omega_n, \pm2\omega_n$  (23).

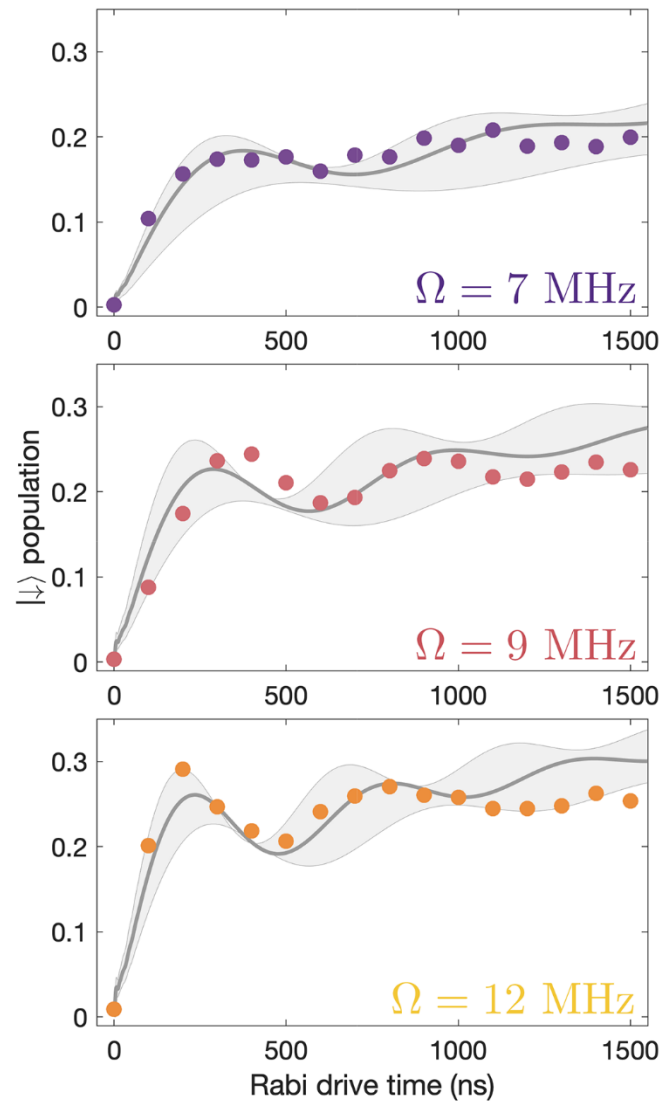


**Fig. 4. Coherent oscillations of a nuclear magnon.** Electronic excited-state  $|\downarrow\rangle$  population (23), measured after a Rabi pulse of  $\tau$  at  $\delta = -2\omega_n = 52$  MHz detuning, at 3.5 T. The carrier Rabi frequency  $\Omega$  is 7, 9, and 12 MHz (23) for measurements shown in the top, middle, and bottom panels, respectively. Solid curves are the corresponding theoretical calculations with  $\eta = 15\%$ , using the same carrier Rabi frequencies. The shaded areas represent a  $\sim\pm 20\%$  deviation in model Rabi frequency.

## Quantum interface of an electron and a nuclear ensemble

D. A. Gangloff, G. Éthier-Majcher, C. Lang, E. V. Denning, J. H. Bodey, D. M. Jackson, E. Clarke, M. Hugues, C. Le Gall and M. Atatüre

published online February 21, 2019

### ARTICLE TOOLS

<http://science.sciencemag.org/content/early/2019/02/20/science.aaw2906>

### SUPPLEMENTARY MATERIALS

<http://science.sciencemag.org/content/suppl/2019/02/20/science.aaw2906.DC1>

### REFERENCES

This article cites 51 articles, 5 of which you can access for free  
<http://science.sciencemag.org/content/early/2019/02/20/science.aaw2906#BIBL>

### PERMISSIONS

<http://www.sciencemag.org/help/reprints-and-permissions>

Use of this article is subject to the [Terms of Service](#)